



OPEN

SUBJECT AREAS:

TOPOLOGICAL
INSULATORSELECTRONIC PROPERTIES AND
MATERIALS

Angle-resolved Photoemission Spectroscopy Study on the Surface States of the Correlated Topological Insulator YbB_6

Received
7 July 2014Accepted
21 July 2014Published
8 August 2014M. Xia^{1*}, J. Jiang^{1*}, Z. R. Ye¹, Y. H. Wang², Y. Zhang³, S. D. Chen², X. H. Niu¹, D. F. Xu¹, F. Chen⁴, X. H. Chen⁴, B. P. Xie¹, T. Zhang¹ & D. L. Feng¹

¹State Key Laboratory of Surface Physics, Department of Physics, and Advanced Materials Laboratory, Fudan University, Shanghai 200433, China, ²Department of Physics and Applied Physics, Stanford University, Stanford, California, 94305, USA, ³Stanford Institute for Materials and Energy Sciences, SLAC National Accelerator Laboratory, 2575 Sand Hill Road, Menlo Park, California 94025, USA, ⁴Department of Physics and Hefei National Laboratory for Physical Science at Microscale, University of Science and Technology of China, Hefei 230026, China.

Correspondence and requests for materials should be addressed to T.Z. (tzhang18@fudan.edu.cn) or D.L.F. (dlfeng@fudan.edu.cn)

* These authors contributed equally to this work.

YbB_6 is recently predicted to be a moderately correlated topological insulator, which provides a playground to explore the interplay between correlation and topological properties. With angle-resolved photoemission spectroscopy, we directly observed almost linearly dispersive bands around the time-reversal invariant momenta $\bar{\Gamma}$ and \bar{X} with negligible k_z dependence, consistent with odd number of surface states crossing the Fermi level in a Z_2 topological insulator. Circular dichroism photoemission spectra suggest that these in-gap states possess chirality of orbital angular momentum, which is related to the chiral spin texture, further indicative of their topological nature. The observed insulating gap of YbB_6 is about 100 meV, larger than that found by theoretical calculations. Our results present strong evidence that YbB_6 is a correlated topological insulator and provide a foundation for further studies of this promising material.

Topological insulator (TI) is a new class of matter with topologically protected surface states that possess unique electronic and spin properties^{1–4}. Recently, how the topological order interplays with the electronic correlation has attracted a lot of theoretical considerations. As materials with significant correlations, the rare-earth borides are interesting with a variety of correlated phenomena including mixed valence, heavy fermion and superconductivity^{5–11}. Especially, samarium hexaboride (SmB_6) has recently been predicted to be a topological Kondo insulator^{12,13}, which fueled intense effort in search for topological orders in correlated systems. Numerous experiments have been performed to identify surface states in SmB_6 (ref. 14–18). Previous angle-resolved photoemission spectroscopy (ARPES) data shows that the bulk states coexist with the surface states with temperature down to 1 K, and the insulating gap of SmB_6 has found to be around 18 meV (ref. 15). Thus, it is important to search for materials with larger insulating gap or cleaner surface states in analogous to the topological SmB_6 .

YbB_6 is a related rare-earth hexaborides which shares the same CsCl type crystal structure with SmB_6 (ref. 19), and is predicted to be a moderately correlated TI with a bulk insulating gap of about 31 meV (ref. 20). With a larger band gap than that of SmB_6 , YbB_6 might be another promising candidate for applications based on topological surface states. However, despite the previous successes of density functional theory in predicting TIs (ref. 2, 21 and 22), the correlations in rare-earth compounds pose challenges to an accurate calculation. For instance, the resistivity of YbB_6 exhibits a bulk metallic behavior²³, inconsistent with the prediction. Therefore, it is crucial to experimentally determine the electronic structure and topological nature of YbB_6 . ARPES is a powerful tool to directly measure the surface and bulk band dispersions and determine the value of topological invariant of three-dimensional TIs (ref. 3, 4 and 16). Furthermore, circular dichroism (CD) of the ARPES data have been shown to be related to the spin textures of the surface states^{15,24–29}.

In this study, we report our ARPES measurements on YbB_6 single crystals. Linearly dispersive bands were observed in its insulating gap around $\bar{\Gamma}$ and \bar{X} with negligible k_z dependences, indicative of their surface origins. The CD of these in-gap states at various photon energies show patterns consistent with the locked spin-

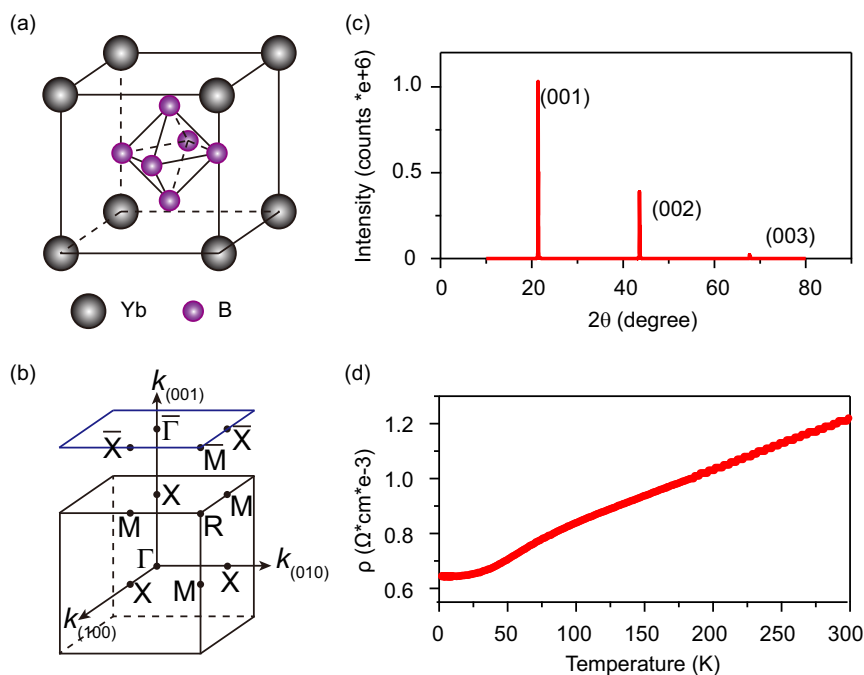


Figure 1 | Crystal structure and Sample characterization. (a) Crystal structure of YbB_6 . (b) Bulk and surface Brillouin zone of YbB_6 and the high symmetry points. (c) X-ray diffraction pattern of YbB_6 single crystals. (d) Resistivity of YbB_6 single crystals measured from 2 K to 300 K.

momentum texture of TIs. The CD pattern of the α band around $\bar{\Gamma}$ shows obvious two-fold symmetry, while the β band around \bar{X} presents anti-symmetric pattern about the $\bar{\Gamma}-\bar{X}$ axis in the surface Brillouin zone (BZ). Moreover, we found that the chemical potential varies up to about 500 meV, from one cleaved surface to another, or sometimes even across the same surface. The bulk bands often coexist with the topological surface states, however, we also identified a

bulk insulating gap of about 100 meV, much larger than predicted²⁰. It is thus possible to tune the chemical potential into such a gap and realize the surface states dominated transport.

Results

Sample characterizations. Sample preparation and experimental details are described in the Methods section. YbB_6 crystallizes in

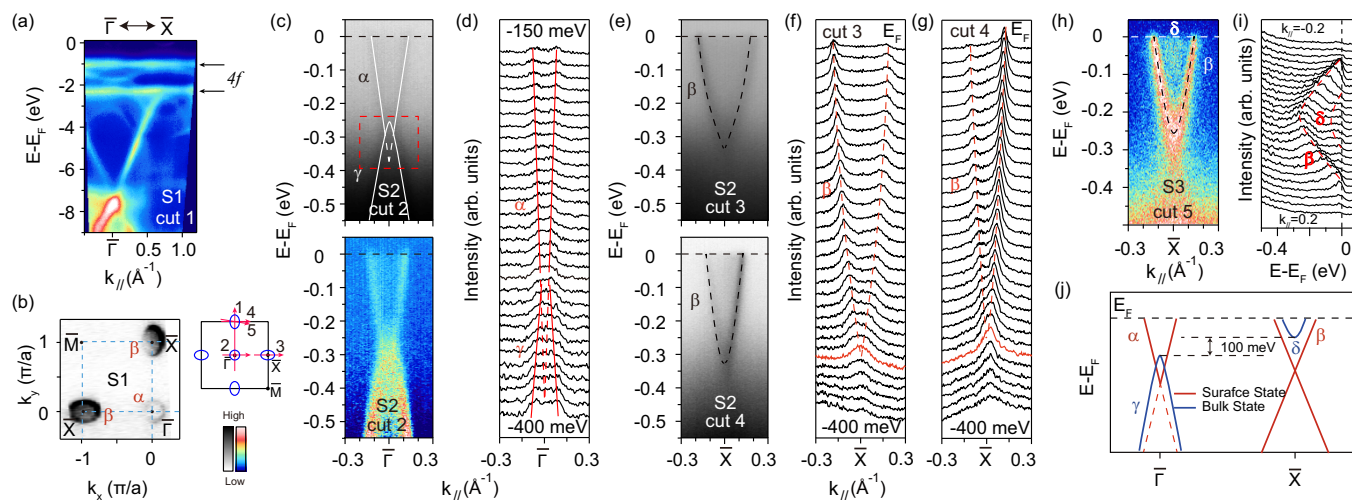


Figure 2 | Valence band structure and low-energy dispersive states of YbB_6 . (a) Photoemission intensity plot showing the valence band structure of YbB_6 . The flat $4f$ bands are marked by the arrows. Data were taken along cut 1 of S1 at 6 K with 33 eV photons in SSRL. (b) Left: photoemission intensity map at E_F taken with 31 eV photons at 6 K in SSRL. The intensity was integrated over a window of $[E_F - 10 \text{ meV}, E_F + 10 \text{ meV}]$. Right: the momentum cuts along which data were taken are marked in the projected two-dimensional BZ. (c) Top: the photoemission intensity plot along cut 2 taken on S2 with 91 eV photons at 18 K in SLS. Bottom: the same data after subtracting a momentum-independent background. The spectra far away from the dispersive region show no momentum dependence and thus taken as the background. The white lines indicate the α and γ bands, the dashed line is extrapolated from the linear dispersion. The red dashed line indicates the overlap of the band bottom of α and band top of γ . (d) The corresponding MDCs along cut 2 within $[E_F - 400 \text{ meV}, E_F - 150 \text{ meV}]$. The red line is the dispersion tracked from the MDC peaks and the red dashed line is extrapolated from the linear dispersion. (e) The photoemission intensity plot on S2 along cut 3 and cut 4 measured with 70 eV photons at 18 K in SLS. (f, g) The corresponding MDCs along cut 3 and cut 4 in panel (e), respectively. The red dashed lines are the dispersions of the β bands. The highlighted MDC in red indicates the possible energy position of the Dirac points. (h, i) The photoemission intensity plot on S3 along cut 5 and its corresponding energy distribution curves (EDCs) taken with 47 eV photons at 20 K in KEK, showing an additional δ band. (j) A schematic of all the bands observed along $\bar{\Gamma}-\bar{X}$ direction.

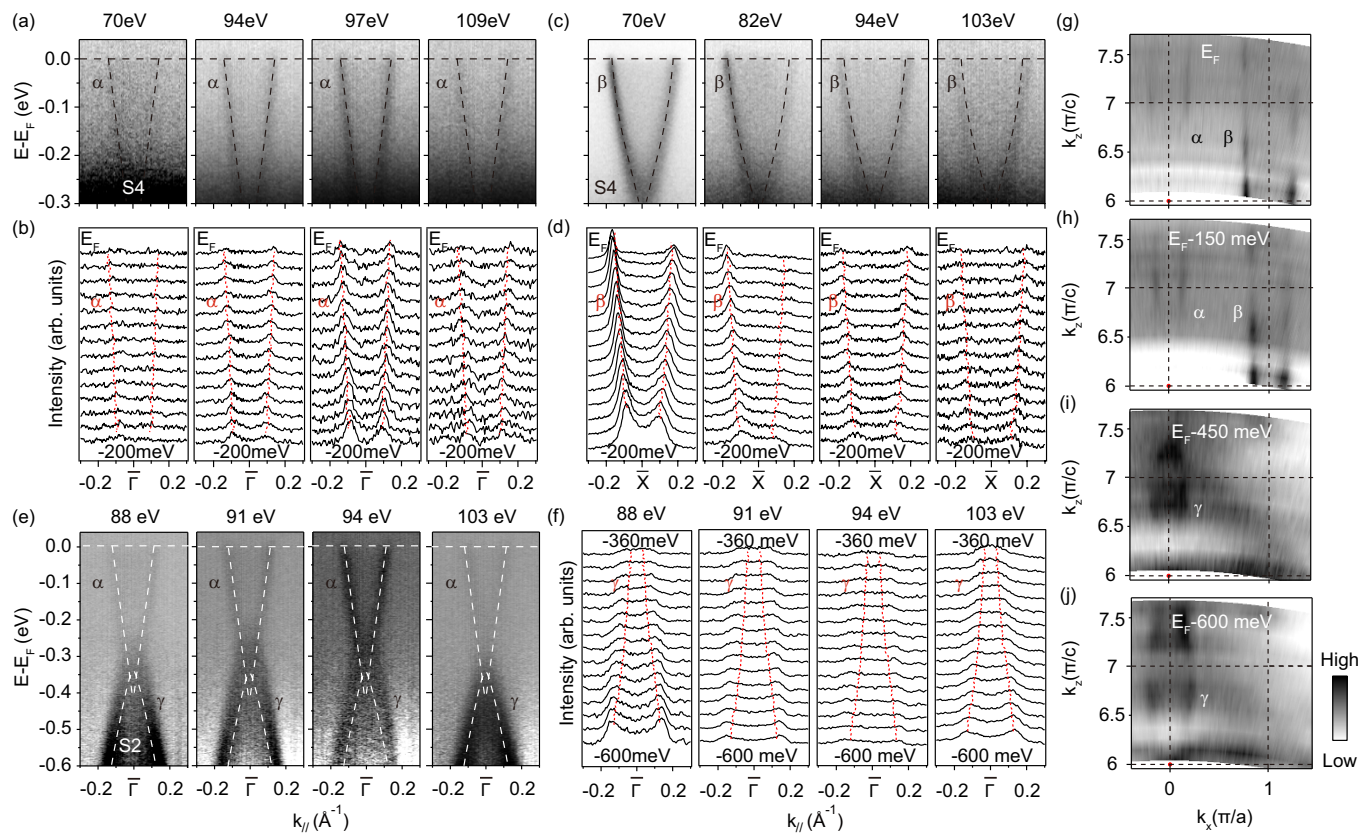


Figure 3 | Photon energy dependence of the α , β and γ bands. (a, b) Photon energy dependence of the photoemission intensity of the α band measured along cut 2 on S4 and its corresponding MDC plots within $[E_F - 200 \text{ meV}, E_F]$. (c, d) The same for the β band as in panel (a) and (b) measured along cut 3 on S4. (e, f) Photon energy dependence of the photoemission intensity of the γ band measured along cut 2 on S2 and its corresponding MDC plots within $[E_F - 600 \text{ meV}, E_F - 360 \text{ meV}]$. The data in panel (e) is subtracted by a momentum-independent background, and thus they are taken as the background. The spectra far away from the dispersive region show no momentum dependence, and thus they are taken as the background. The red dashed lines in panel (b), (d) and (f) are fitted dispersions with 94 eV data of the α and β bands and with 103 eV data of the γ band, respectively, and overlaid them onto the data of other photon energies. The white dashed lines in panel (e) are extracted from the 103 eV data indicating the α and γ bands, and overlaid them on top of data with other photon energies. (g–j) Photoemission intensity plots in the k_z - k_x plane at E_F , $E_F - 150 \text{ meV}$, $E_F - 450 \text{ meV}$, $E_F - 600 \text{ meV}$, respectively. The intensity was integrated over a window of $[E_F - 10 \text{ meV}, E_F + 10 \text{ meV}]$. The red dashed lines indicate the dispersions of the α , β and γ bands along k_z direction. Data were taken at 18 K in SLS.

the cubic $Pm\bar{3}m$ space group and can be considered as the CsCl-type structure with the Yb ions and the B_6 octahedra being located at the corner and the body center of the cubic lattice, respectively, as shown in Fig. 1(a). Figure 1(b) shows the bulk BZ together with the projected surface BZ. The high symmetry points we used are indicated in this panel. The X-ray diffraction pattern presented in Fig. 1(c) indicates a high sample quality of our single crystal and the natural surface is the (001) surface. The resistivity of YbB₆ single crystal shows a metallic behavior down to 2 K (Fig. 1(d)), consistent with previous report in ref. 23, which can be further understood by the coexistence of the bulk band with the surface states that will be discussed below.

Bulk valence bands and the linear-dispersive states. Figure 2(a) shows the photoemission intensity of YbB₆ on sample 1 (S1) over a large energy scale, the non-dispersive Yb $4f$ bands are located at around 1 eV and 2.3 eV below Fermi energy (E_F). They correspond to the $^2F_{7/2}$ and $^2F_{5/2}$ multiplets of the Yb $^{2+}$ $4f^4 \rightarrow 4f^3$ final states based on the LDA calculation²⁰. The energy difference between the two multiplets is 1.3 eV, consistent with the calculation. However, the energy positions of these $4f$ bands are deeper than that calculated in Ref. 20, suggesting correlation effects need to be reconsidered in calculation. In addition, some dispersive features are resolved in the low energy range, which may mostly originate from the Yb $5d$ orbitals²⁰.

The photoemission intensity map at E_F on S1 is shown in Fig. 2(b). An elliptical Fermi pocket located around \bar{X} and a circular Fermi pocket around $\bar{\Gamma}$ are clearly observed. The photoemission intensity distribution across $\bar{\Gamma}$ taken on sample 2 (S2) is plotted in Fig. 2(c), together with a background subtracted one to visualize the dispersions more clearly. There is an electron-like band (referred to as α), forming the circular Fermi pocket in Fig. 2(b). In Fig. 2(e), another electron-like band is observed around \bar{X} (referred to as β), forming the elliptical Fermi pocket.

Both the α and β bands exhibit almost linear dispersions as can be seen from their momentum distribution curves (MDCs) in Figs. 2(d), 2(f) and 2(g). The α band extrapolates to cross at about 380 meV below E_F . There is also a γ band below the α band. However, the band bottom of α overlaps with the band top of γ in certain energy range as highlighted in Fig. 2(c). This observation, together with the very different intensities of γ and α , indicates that γ is not the lower cone of α , if there is a Dirac point as predicted²⁰. Due to the low intensity of the α band and the interference of the strong γ band, the lower cone is hardly resolved, if any.

The β band also seems to cross at about 320 meV below E_F by tracking its linear dispersion, but the predicted lower cone could not be distinguished either, due to the strong residual intensity of the flat $4f$ bands. The δ band is only observed within a narrow photon energy range [e.g. 47 eV in Fig. 2(h)] with its band bottom around

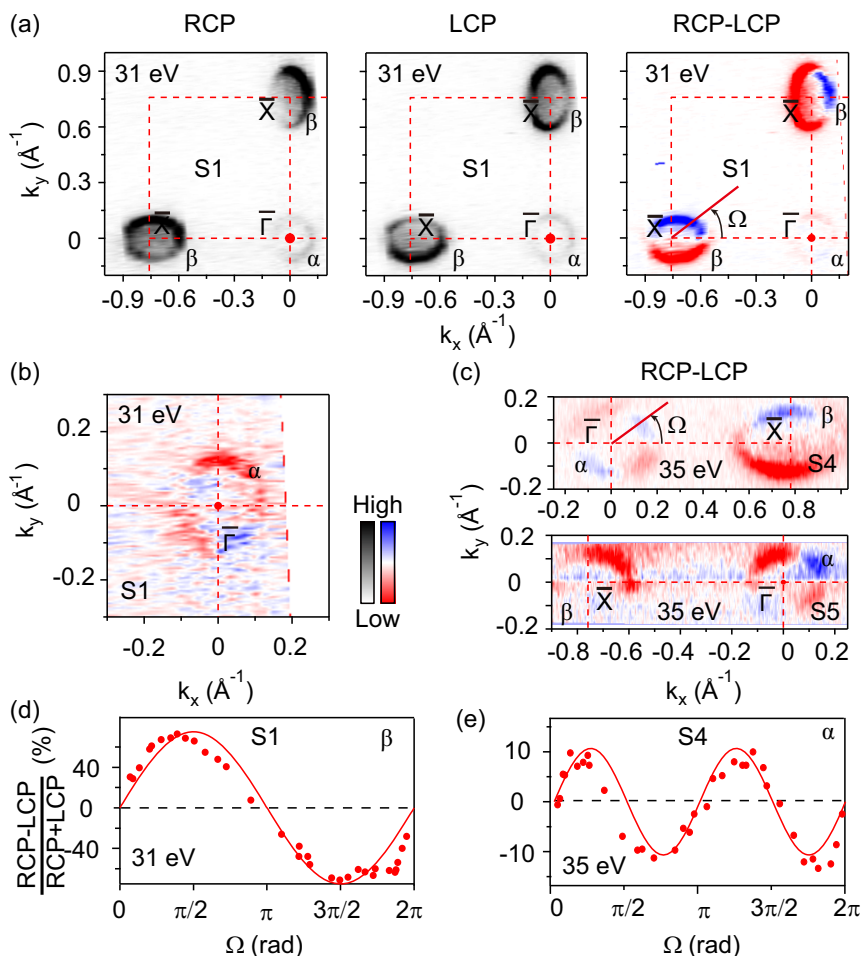


Figure 4 | Circular Dichroism of the surface states around $\bar{\Gamma}$ and \bar{X} . (a) Fermi surface maps of YbB₆ taken with RCP, LCP light and their difference (RCP-LCP) of S1. The intensity was integrated over a window of $[E_F - 10 \text{ meV}, E_F + 10 \text{ meV}]$. (b) The RCP-LCP data around $\bar{\Gamma}$ enlarged from panel (a). (c) Top: CD result of S4 (top) and S5 (bottom) measured with 35 eV photons showing the right \bar{X} pocket and the left \bar{X} pocket, respectively. (d) The CD values taken along the left pocket around \bar{X} in panel (a) of S1 as a function of the polar angle Ω . Ω is defined within panel (a) respect to \bar{X} . (e) The same as that in panel (d) to show the CD of α pocket taken on S4, where Ω is defined within panel (c) respect to $\bar{\Gamma}$. The red solid curves in panel (d) and (e) are sine function fits of the data. The 31 eV data were taken at 6 K in SSRL and the 35 eV data were taken at 18 K in SLS.

−80 meV measured on sample 3 (S3). The band bottom of β in S3 is around −250 meV, different from that in S2, which may be caused by the difference in their chemical potentials. Figure 2(j) is the schematic of all the low-lying energy bands resolved along $\bar{\Gamma} - \bar{X}$ direction.

Photon energy dependence of the linear-dispersive bands. Photon energy dependent ARPES experiments have been performed to examine how the α , β and γ bands vary with k_z . The photoemission intensity distributions taken with different photon energies are presented in Fig. 3. One can see that, for both α and β bands, although the spectral weight varies with photon energy due to photoemission matrix element effects, the dispersions of them remain unchanged. Figures 3(a) and 3(b) show the photoemission intensity distributions across $\bar{\Gamma}$ on sample 4 (S4) together with their corresponding MDCs. We fitted the dispersion of the α band taken with 94 eV photons and overlaid it onto the data taken with several other photon energies, which clearly show that the dispersion of α is k_z independent. The same process has been done to the β band in Figs. 3(c) and 3(d), which also show no k_z dependence. More data under other photon energies can be found in the Supplementary Information (SI).

However, in Figs. 3(e) and 3(f), when we overlaid the dispersion of γ extracted from the MDCs taken with 103 eV photons on top of the data taken with several other photon energies, there are clear mis-

matches. That is, the γ band disperses with k_z , indicative of its bulk origin. Furthermore, the dark interior of intensity envelopes of the γ band in Fig. 3(e) is likely due to its dispersion along k_z and the poor k_z resolution in ARPES measurements with vacuum ultraviolet photons. Similar behavior has been reported for a bulk band in SmB₆ (ref. 15). The band top of the valence band (γ band) observed here is located at the $\bar{\Gamma}$ point, which is quite different from the theoretical calculation where the top of the valence band is around the \bar{X} point²⁰. We also note that our observation of the γ band is consistent with another ARPES data reported recently³⁰. Such a sharp contradiction between the experiment and theoretical calculation calls for further understanding of YbB₆.

Moreover, the k_z - k_x intensity plots at E_F , E_F -150 meV, E_F -450 meV, E_F -600 meV are shown in Figs. 3(g)-3(j) assuming the chemical potential to be 15 eV, which clearly show the evolution with k_z of these bands. The crossings of the α band and the β band remain unchanged (Figs. 3(g) and 3(h)), consistent with the two-dimensional nature of them. However, the data at E_F -450 meV and E_F -600 meV in Figs. 3(i) and 3(j) clearly show the variation of the γ band with different k_z 's. The evident dispersion along k_z further indicates its bulk origin. This assignment is consistent with a recent bulk sensitive soft X-ray ARPES study on YbB₆ (ref. 30).

The δ band is only observed in certain photon energies, due to different cross-section of this band. The lineshape of the δ band is

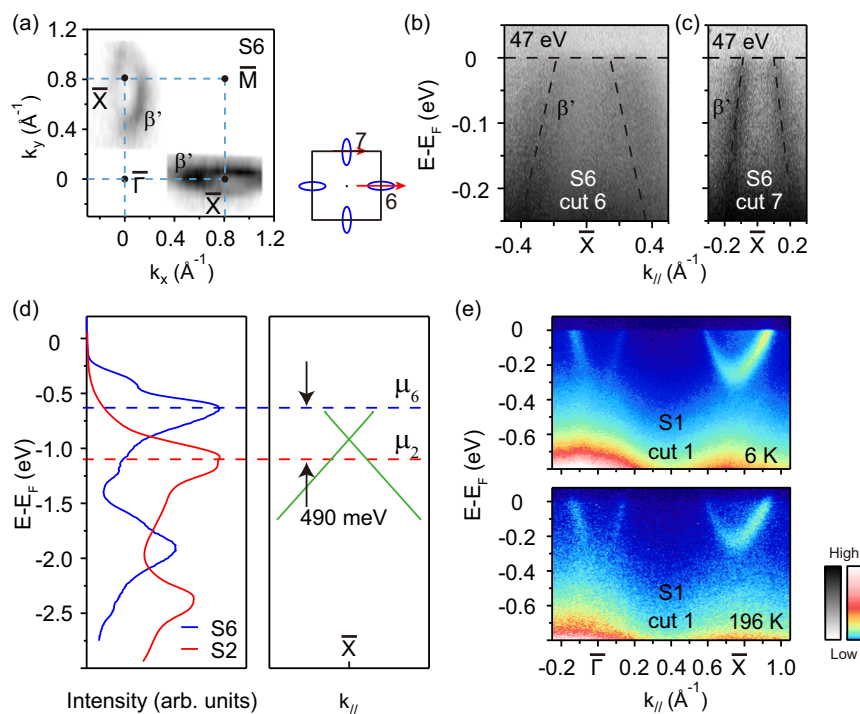


Figure 5 | Hole-like surface in YbB_6 and temperature dependent electronic structure of electron-like surface in YbB_6 . (a) Left: Photoemission intensity map of S6 with hole-like pockets. The intensity was integrated over a window of $[E_F - 10 \text{ meV}, E_F + 10 \text{ meV}]$. Right: the momentum cuts along which the data were taken are marked in the projected two-dimensional BZ. (b, c) Two photoemission intensity plots taken along cut 6 and cut 7 indicated in panel (a) by the blue arrows, respectively. The hole-like dispersions are indicated by the dashed lines. Data were taken on S6 at 20 K with 47 eV photons in KEK. (d) A schematic plot to show the chemical potential shift in different surfaces and the integrated EDCs of the two different surface to compare the different chemical potential. μ_2 and μ_6 refer to the chemical potential of the two different cleaved surfaces of S2 and S6. (e) The photoemission intensity data taken along $\bar{\Gamma}-\bar{X}$ direction at 6 K and 196 K, respectively. Data were taken on S1 at SSRL with 31 eV photons.

hardly resolved due to its bulk origin and poor k_z resolution, which results in a bright interior of intensity envelopes of the δ band. Thus the δ band should be the bulk conduction band, which can well explain the metallic resistivity behavior in YbB_6 (see Fig. 1(d)). As the band bottom of the δ band in S3 is around -80 meV , the band bottom of δ in S2 should be around -150 meV , due to the 70 meV difference in chemical potential between these two samples (see SI). Moreover, since the band top of γ in the 91 eV data of S2 locates at around -250 meV [Fig. 2(c)], the bulk band gap of YbB_6 is likely to be about 100 meV, as illustrated in Fig. 2(j). This determined gap size is much larger than the theoretical prediction of only 31 meV (ref. 20), which suggests the correlation effects need to be better treated in the calculations.

The circular dichroism of the linear-dispersive bands. The chirality of spin and orbital angular momentum (OAM) is another remarkable hallmark of the topological surface state, since both of them are interlocked and rotate with the electron momentum, so that the total angular momentum is conserved. To further explore the topological nature of these surface states, we conducted CD-ARPES experiment, which probes the chirality of the OAM^{15,28}.

The Fermi surface maps of S1 measured under right-handed circular polarized (RCP) light and left-handed circular polarized (LCP) light are shown in Fig. 4(a), together with their difference (referred to as RCP-LCP). The CD of the β pocket shows an anti-symmetric pattern about the $\bar{\Gamma}-\bar{X}$ axis in the surface BZ. The enlarged CD image near $\bar{\Gamma}$ is shown in Fig. 4(b). Although its intensity is much weaker than that of the β pocket, we can see that the symmetry of the α pocket becomes two-fold, which is different from the anti-symmetric CD pattern of the β pocket. Such symmetries are confirmed by another set of data with more statistics in the top panel of Fig. 4(c), which was measured on S4 with 35 eV photons, showing

the α pocket and the right β pocket. The bottom panel in Fig. 4c is measured on sample 5 (S5), under the same condition as S2, but presents the left β pocket. Clearly, all the CD patterns exhibit an inversion symmetry with respect to $\bar{\Gamma}-\bar{X}$.

Moreover, we observe a sign change between the 31 eV and 35 eV CD data in both the α and β pockets. This simultaneous sign change can be attributed to a final-state effect of the CD-ARPES as reported in Bi_2Se_3 (ref. 24). In Figs. 4(d) and 4(e), we plot the representative CD distributions around the α and β pockets. Both of them can be well fitted by a sine function, however, the period for β is 2π , while that for α is π . The reductive period of the α band, or the two-fold symmetric CD pattern needs further investigation, but similar behaviors were attributed to the coupling to bulk states in Bi_2Se_3 and Bi_2Te_3 (ref. 29, 31–33). Despite the intriguing symmetry, the CD results do suggest that the chirality of OAM exist in both the α and β bands, indicating that they might possess helical spin textures.

From the data above, the surface nature and the possible topological origin of the α and β bands have been established. We also note that there is one Fermi pocket around $\bar{\Gamma}$ and two Fermi pockets around \bar{X} in the surface BZ, the total number of surface states is odd, thus the whole system should be topologically non-trivial. This is remarkably consistent with the theoretical prediction that YbB_6 is a Z_2 TI (ref. 20).

The variation of surface chemical potential. We found that the chemical potential varies during different samples. In most cases the variation is within 100 meV and the band structure is similar as discussed above. But sometimes, we observed very different, hole-like pocket around \bar{X} , referred to as β' in Figs. 5(a)–5(c). The electron-like Fermi pocket and the hole-like Fermi pocket can be even observed in different regions of the same sample, which may be due to inhomogeneous doping of the sample or different surface



conditions. The chemical potential of the sample with hole-like pockets (S6) differs 490 meV from that of S2 with electron-like pockets, indicated by the shift of the 4*f* bands between these two samples shown in Fig. 5(d). Since the linear extrapolation of β' in S6 leads to a crossing at around 180 meV above E_F and the crossing point of β is located at around 320 meV below E_F , the energy position of the crossing point shifted about 500 meV. This is consistent with the 490 meV shift of the 4*f* bands within error bar, indicating that β' could be the lower half of the possible Dirac cone of β . The slope of β near its crossing point and the slope of β' are nearly same with only 4% difference, further support they are from one Dirac cone. Around $\bar{\Gamma}$, on the other hand, we did not resolve the band below the crossing of α , which could be concealed by the bulk band γ .

Temperature dependence of the electronic structure. The observed surface states in YbB₆ are robust against the change of temperature from 6 K to 196 K [Fig. 5(e)]. This is consistent with the theoretical calculations which show that YbB₆ is a moderately correlated insulator but not a Kondo insulator²⁰.

Conclusion. To summarize, we have obtained a comprehensive understanding of the electronic structure of YbB₆ from ARPES. We directly observed several linearly dispersive bands within the insulating gap of YbB₆ that show negligible k_z dependence. The CD-ARPES data indicate well-defined helical spin texture of the surface states. These results suggest that YbB₆ is a TI. We note that the sensitivity of chemical potential reported here also implies its tunability. If the chemical potential can be tuned into the 100 meV insulating gap, the topological surface state can be exploited in applications without the interference from the bulk states.

Methods

Sample synthesis. High quality YbB₆ single crystals were synthesized by the Al-flux method. A chunk of Yb together with the powders of Boron and Al were mixed with a ratio of 1:6:400 and heated to 1773 K in an alumina crucible in the argon atmosphere, then maintained at 1773 K for about 2 days before slowly cooling down to 873 K at a rate of 5 K per hour.

ARPES measurement. ARPES measurements were performed at the SIS beamline of Swiss Light Source (SLS) and Beamline 5-4 of Stanford Synchrotron Radiation Lightsource (SSRL), both equipped with a Scienta R4000 electron analyzer, and beamline 28A of Photon Factory, KEK, equipped with a Scienta SES-2002 electron analyzer. The angular resolution was 0.3° and the overall energy resolution was better than 15 meV depending on the photon energy. The samples were cleaved *in situ* along the (001) plane and measured under ultra-high vacuum below 5×10^{-11} torr.

- Hasan, M. Z. & Kane, C. L. Colloquium: topological insulators. *Rev. Mod. Phys.* **82**, 3045 (2010).
- Zhang, H. J. *et al.* Topological insulators in Bi₂Se₃, Bi₂Te₃ and Sb₂Te₃ with a single Dirac cone on the surface. *Nat. Phys.* **5**, 438 (2009).
- Chen, Y. L. *et al.* Experimental realization of a three-dimensional topological insulator, Bi₂Te₃. *Science* **325**, 178 (2009).
- Hsieh, D. *et al.* A tunable topological insulator in the spin helical Dirac transport regime. *Nature* **460**, 1101 (2009).
- Kato, Y. *et al.* Buffer-layer-enhanced growth of a single-domain LaB₆ (100) epitaxial thin film on a MgO (100) substrate via pulsed laser deposition. *Journal of Crystal Growth* **330**, 39–42 (2011).
- Menth, A. *et al.* Configuration of Sm in SmB₆. *J. Appl. Phys.* **40**, 1006 (1969).
- Ignatov, M. I. *et al.* Anomalous thermopower in heavy-fermion compounds CeB₆, CeAl₃, and CeCu_{6-x}Au_x. *J. Exp. Theor. Phys.* **105**, 58 (2007).
- Mori, Y. *et al.* Photoemission and BIS of RB₆ (R = rare earth element). *Physica B* **186–188**, 66–69 (1993).
- Fisk, Z., Schmidt, P. H. & Longinotti, L. D. Growth of YB₆ Single Crystals. *Mater. Res. Bull.* **11**, 1019 (1976).
- Kim, D. J., Grant, T. & Fisk, Z. Limit Cycle and Anomalous Capacitance in the Kondo Insulator SmB₆. *Phys. Rev. Lett.* **109**, 096601 (2012).
- Late, D. J. *et al.* Some aspects of pulsed laser deposited nanocrystalline LaB₆ film: atomic force microscopy, constant force current imaging and field emission investigations. *Nanotechnology* **19**, 265605 (2008).
- Dzero, M., Sun, K., Galitski, V. & Coleman, P. Topological Kondo Insulators. *Phys. Rev. Lett.* **104**, 106408 (2010).
- Lu, F., Zhao, J. Z., Weng, H. M., Fang, Z. & Dai, X. Correlated topological insulators with mixed valence. *Phys. Rev. Lett.* **110**, 096401 (2013).

- Takimoto, T. SmB₆: A Promising Candidate for a Topological Insulator. *J. Phys. Soc. Jpn.* **80**, 123710 (2011).
- Jiang, J. *et al.* Observation of possible topological in-gap surface states in the Kondo insulator SmB₆ by photoemission. *Nat. Commun.* **4**, 3010 (2013)
- Neupane, M. *et al.* Surface electronic structure of the topological Kondo Insulator candidate correlated electron system SmB₆. *Nat. Commun.* **4**, 2991 (2013).
- Xu, N. *et al.* Surface and bulk electronic structure of the strongly correlated system SmB₆ and implications for a topological Kondo insulator. *Phys. Rev. B* **88**, 121102 (2013).
- Wolgast, S. *et al.* Low-temperature surface conduction in the Kondo insulator SmB₆. *Phys. Rev. B* **88**, 180405 (2013).
- Apra, A. *et al.* Nanosized rare-earth hexaborides: Low-temperature preparation and microstructural analysis. *Solid State Sciences* **21**, 32–36 (2013).
- Weng, H. M., Zhao, J. Z., Wang, Z. J., Fang, Z. & Dai, X. Topological Crystalline Kondo Insulator in Mixed Valence Ytterbium Borides. *Phys. Rev. Lett.* **112**, 016403 (2014).
- Bernevig, B. A., Hughes, T. L. & Zhang, S. C. Quantum Spin Hall Effect and Topological Phase Transition in HgTe Quantum Wells. *Science* **314**, 1757 (2006).
- König, M. *et al.* Quantum Spin Hall Insulator State in HgTe Quantum Wells. *Science* **318**, 766 (2007).
- Tarascon, J. M. *et al.* Magnetic and transport properties of pure and carbon-doped divalent RE hexaboride single crystals. *J. Appl. Phys.* **51**, 574 (1980).
- Scholz, M. R. *et al.* Reversal of the Circular Dichroism in Angle-Resolved Photoemission from Bi₂Te₃. *Phys. Rev. Lett.* **110**, 216801 (2013).
- Wang, Y. H. *et al.* Observation of a Warped Helical Spin Texture in Bi₂Se₃ from Circular Dichroism Angle-Resolved Photoemission Spectroscopy. *Phys. Rev. Lett.* **107**, 207602 (2011).
- Zhu, Z.-H. *et al.* Layer-By-Layer Entangled Spin-Orbital Texture of the Topological Surface State in Bi₂Se₃. *Phys. Rev. Lett.* **110**, 216401 (2013).
- Park, Cheol-Hwan & Louie, Steven G. Spin Polarization of Photoelectrons from Topological Insulators. *Phys. Rev. Lett.* **109**, 097601 (2012).
- Park, S. R. *et al.* Chiral Orbital-Angular Momentum in the Surface States of Bi₂Se₃. *Phys. Rev. Lett.* **108**, 046805 (2012).
- Wang, Y. H. & Gedik, N. Circular dichroism in angle-resolved photoemission spectroscopy of topological insulators. *Phys. Status Solidi RRL* **7**, No. 1–2, 64–71 (2013).
- Xu, N. *et al.* Surface vs bulk electronic structures of a moderately correlated topological insulator YbB₆ revealed by ARPES. arxiv: 1405.0165.
- Mirhosseini, H. & Henk, J. Spin Texture and Circular Dichroism in Photoelectron Spectroscopy from the Topological Insulator Bi₂Te₃: First-Principles Photoemission Calculations. *Phys. Rev. Lett.* **109**, 036803 (2012).
- Jung, W. *et al.* Warping effects in the band and angular-momentum structures of the topological insulator Bi₂Te₃. *Phys. Rev. B* **84**, 245435 (2011).
- Bahramy, M. S. *et al.* Emergent quantum confinement at topological insulator surfaces. *Nature Communications* **3**, 1159 (2012).

Acknowledgments

We thank Dr. M. Shi and Dr. N. Xu at SLS and Dr. K. Ono and Dr. N. Inami at KEK. This work is supported in part by the National Science Foundation of China and National Basic Research Program of China (973 Program) under the grant Nos. 2012CB921402, 2011CB921802, 2011CBA00112. SSRL is operated by the U. S. DOE Office of Basic Energy Science.

Author contributions

M.X., J.J., Z.R.Y., X.H.N., D.F.X., Y.Z., S.D.C. and B.P.X. performed ARPES measurements. F.C. and X.H.C. grew the samples and conducted sample characterization measurements. M.X., J.J., Y.H.W., T.Z. and D.L.F. analyzed the ARPES data. M.X., J.J., T.Z. and D.L.F. wrote the paper. D.L.F. and T.Z. are responsible for the infrastructure, project direction and planning.

Additional information

Supplementary information accompanies this paper at <http://www.nature.com/scientificreports>

Competing financial interests: The authors declare no competing financial interests.

How to cite this article: Xia, M. *et al.* Angle-resolved Photoemission Spectroscopy Study on the Surface States of the Correlated Topological Insulator YbB₆. *Sci. Rep.* **4**, 5999; DOI:10.1038/srep05999 (2014).



This work is licensed under a Creative Commons Attribution-NonCommercial-NoDerivs 4.0 International License. The images or other third party material in this article are included in the article's Creative Commons license, unless indicated otherwise in the credit line; if the material is not included under the Creative Commons license, users will need to obtain permission from the license holder in order to reproduce the material. To view a copy of this license, visit <http://creativecommons.org/licenses/by-nc-nd/4.0/>